American Journal of
Nanotechnology & Nanomedicine

Research Article

Revisiting Water Molecule Interactions with Hydrogenated Nanodiamonds: Towards Their Direct Quantification in Aqueous Suspensions

Ivana Chaux-Jukic[1,2*], Cheikh Benoit Faye[2], Philippe Bergonzo[3], Romain Grall[2], Sylvie Chevillard[2], Nicolas Ugolin[2]

[1]*BIP3D, 7 rue la Boissiere, 92260 Fontenay-aux-Roses, France*

[2]*CEA, DRF, IRCM, SREIT, Laboratory of Experimental Cancerology, 18 route du panorama, 92265 Fontenay-aux-Roses, France*

[3]*CEA, LIST, F-91191 Gif-sur-Yvette, France*

***Address for Correspondence:** Ivana Chaux-Jukic, BIP3D, 7 rue la Boissiere, 92260 Fontenay-aux-Roses, France, ORCID iD: https://orcid.org/0000-0003-3540-6687, E-mail: ivana.jukic@hotmail.com/ ivana.jukic@cea.fr

Submitted: 19 November 2019 **Approved:** 16 December 2019 **Published:** 19 December 2019

Cite this article: Chaux-Jukic I, Faye CB, Bergonzo P, Grall R, Chevillard S, et al. Revisiting Water Molecule Interactions with Hydrogenated Nanodiamonds: Towards Their Direct Quantification in Aqueous Suspensions. Am J Nanotechnol Nanomed. 2019; 2(1): 014-022.

ISSN: 2644-0083

ABSTRACT

Current findings on interactions of water molecules with Hydrogenated Nanodiamonds (H-ND) are still unclear. Through an unusual use of dimethyl sulfoxide, this study by Raman spectroscopy presents a model of the structuration of water molecules surrounding the H-ND. The hydration hereby demonstrated is carried out by direct hydrogen bonds between at least one electron doublet of the oxygen atom from the water molecule and the hydrogen atom from the H-ND surface. These hydrogen bonds at the H-ND-water interface are stabilized by other hydrogen bonds between these water molecules bound to the H-ND. These water molecules in the immediate proximity of H-ND strongly bonded to the H-ND are not removed in the environment with a moderate dimethyl sulfoxide concentration, while the other hydrogen bonds linking only the water molecules are displaced. This property offers a new quantification strategy for H-ND in aqueous suspensions.

INTRODUCTION

Nanodiamonds (ND) elicit particular interests for biological applications. However, among inherent issues that govern not only their dispersibility [1,2] in stable colloids but also their biological internalization and effects on tissues and cells [3,4], the surface termination is one of the key issues that requires particular attention.

When their surface termination is well controlled, ND of average diameter inferior to 20 nm exhibit advantageous physicochemical properties such as; a good colloidal stability in aqueous suspensions, a capacity of surface functionalization by biomolecules, as well as low toxicity rates [3-5]. Because of these qualities the ND excite particularly the scientific community for their potential in biomedical applications [6-8]. These ND properties are essentially the result of a surface chemistry combined to a great specific surface to volume ratio [9,10].

Amongst the existing surface chemistries [11], Hydrogenated ND (H-ND) present a particular interest, more precisely, in radiotherapy, due to their radio-enhancing properties. Indeed, the *in-vitro* tests on radio-resistant cell lines, applying a concomitant exposure of H-ND and ionizing radiation have demonstrated a remarkable efficiency [3]. However, during the preparation of H-ND suspensions, a random H-ND fraction precipitates [12], which leads to uncertain estimations of remaining H-ND density in suspension. Therefore, it is crucial to finely quantify the H-ND in aqueous suspensions, to determine a quantity sufficient for the H-ND optimal efficiency without toxic events *in vitro* or *in vivo*.

However, among the commonly used methods for H-ND characterization, as for example, Fourier Transform Infrared Spectroscopy (FTIR) [13-15] or Raman spectroscopy [8,11,16,17], etc., none of them allows the quantification of H-ND colloidal fraction directly in aqueous suspensions. Generally, indirect analysis may be performed by pre-concentrating the suspension on a filter, combining the nanoparticles with a specific calibrator metal or drying the suspension before a spectroscopic analysis. However, the concentration of nanoparticles obtained by these methods of analysis remains merely approximate and does not correspond to the real concentration of nanoparticles in the analyzed suspension.

Moreover, in Raman spectroscopy, the difficulty of analyzing H-ND directly in a liquid environment results from the interference between the vibrational frequency of the C-C sp^3 bond in diamonds, observed in a solid matrix at 1330 cm^{-1} [18-21] and the vibrational frequencies of water molecules [22,23] around this spectral area. Consequently, this issue forbids all fine identification or quantification of H-ND in an aqueous matrix.

Here, beyond the possibility to provide better insights on the mechanisms set off by ND hydrogen surface termination, we propose a very innovative method that will enable a direct quantitative determination of H-ND in aqueous suspensions. These calculations are brought through the analysis of the alterations in spectroscopic properties of water molecules interacting with H-ND in a water/Dimethyl Sulfoxide (DMSO) aqueous suspensions.

EXPERIMENTAL

Hydrogenated nanodiamonds

Two kinds of H-ND have been used in this study. The first batch of H-ND has been provided by Cardiff Diamond Foundry. H-ND have an average size of 15 nm with a ζ-potential between 49 and 63 mV. The H-ND were prepared, put in suspension at 2 mg/ml and characterized as reported in Oliver AW, et al. [5].

A second batch of H-ND has been provided by Diamond Sensor Laboratory (CEA, Saclay). This batch is of average size of 20 nm with a ζ-potential between 45 and 57 mV. They were prepared put in suspension at 1.8 mg/ml and characterized as reported in Girard, et al. [14]. A representative Raman spectrum of these batches is shown in results.

Raman Spectrometer

Serstech 100 Indicator Raman spectrometer is used for the analysis of H-ND suspension. It is composed of a class 3B laser, with an excitation wavelength of 785 nm and a maximum power of 300 mW. The spectral width goes from 400 to 2300 cm^{-1} with a spectral resolution of 10 cm^{-1}. The detector integrated in the spectrometer is a linear sensor functioning as a Charge Coupled Device (CCD). The instrument is calibrated with [5,12] 50% aqueous DMSO solutions, as well as with a range of H-ND suspensions in corresponding DMSO aqueous solutions.

The Raman laser presents a Gaussian beam of 1mm of average diameter. The diameter of the analysis cuvette is 1cm. With low absorbance of water and the DMSO at 750nm (including the DMSO/water mixture solutions), the attenuation of laser power crossing the cuvette is negligible. The same is also true for ethanol/water solutions. [24] Hence, the power delivered by the laser in a given volume unit of the analysis cuvette may be considered as identical, regardless its position in the cuvette, therefore, a maximum of 300mW/3.4mm^2 (300mW/3.4x$10^{12}$$nm^2$) or 9.5x$10^{-5}$$nW/nm^2$.

However, depending on the concentration of H-ND in suspensions there is an increasing masking effect of the received laser power. This masking effect depends on 1) the distance of the particle from the cuvette side of laser beam's impact and 2) the concentration of H-ND in the suspension. The bigger the distance and the higher the concentration of the particles, the more important the masking effect is.

For the same volume unit in the cuvette, the exposure depends directly on particles' size and concentration. When the size of the particles is homogenous in the cuvette, after agitation, the average power received by the particles in a volume unit, and the Raman signal associated to the same element of volume unit, become dependent only on the particle concentration in that volume unit, since all other elements are a constant.

Normalization methods

The Raman signal has been demonstrated by normalizing the spectrum intensities to one peak intensity. The normalization of Raman spectra for suspensions with DMSO in water is realized with the intensity of DMSO Methyl Group ($-CH_3$) at 950cm^{-1}. For suspension with DMSO in ethanol the peak intensity of the C-C-O vibrational frequency group at 428 cm^{-1} has been used for the normalization. The vibrational frequencies of these normalization peaks are unaffected by the experimental environment.

Sample preparation

All of the analyzed suspensions, have been obtained by taking an aliquot in the initial suspension and diluting in different suspensions to final percentages of 5%, 12%, 50% of DMSO in ultrapure water or suspensions with a 12% DMSO in ethanol.

Selection of quantification relevant frequencies

To determine the relevant frequencies whose spectroscopic signal represents a linear dependency regarding H-ND suspensions concentrations, the spectroscopic intensity measured for each frequency at different H-ND concentrations is plotted in relation to the mentioned H-ND concentrations. A linear regression coefficient has been calculated for each graph. The frequencies have then been ranked in a decreasing order of the linear regression coefficient. The top five of the ranking presents the best linearity between the spectroscopic signal and the H-ND suspension concentration. The measurements being realized in suspensions; the Raman signal is averaged by the Brownian motion of particles. The resulting signals present a Gaussian distribution such as shown in figure 9. The value retained for the intensity measuring is the width at half maximum of the peak.

Phase exchange sample preparations

The aqueous phase in the experiments is ultrapure water. The aliphatic phase is an oil composed of 70% Glyceryl Trilinoleate, 19% Glyceryl Trioleate, 6% Glyceryl Tripalmitate and 5% Glyceryl Tristearate. The perfluoroalkane phase is tetradecafluorohexane. Representative image of phase exchange experiments is shown in results.

RESULTS AND DISCUSSION

The Raman spectroscopy analyses of H-ND in a solid matrix, give the vibrational frequencies of C-C sp^3 bonds characteristic for diamonds at around 1330 cm^{-1} [18-21,25,26]. In some H-ND samples, a C-C sp^2 bond vibrational frequency at around 1650 cm^{-1} may be observed, suggesting graphene presence on the H-ND surface [27,28]. When analyzing ND in a solid matrix by Raman spectroscopy, the peak corresponding to C-C sp^3 at around 1330 cm^{-1} is used for diamond identification and quantification. When in a solid matrix, the density of nanoparticles is defined only by the space they occupy, more specifically, by the form and the size of the given particle. In aqueous suspensions, this type of analysis is not directly quantitative because the volume of an analyzed suspension is very low. Drying these suspensions for a solid-state analysis can lead to material losses or measurement artifacts, which, unfortunately, excludes this solid-state method for measurements in aqueous suspensions. Additionally, the quantity of observed particles in suspensions is proportional to their density (particle concentration in a suspension), which does not depend on their size or shape.

The main challenge is how to make the Raman analysis quantitative directly for H-ND suspensions and thus which spectral line(s) in an aqueous matrix should be relevant. Importantly, in an aqueous environment, the C-C sp^3 diamond signal at around 1330cm^{-1} is blurred by the Raman signal of water molecules observed in the same region. Indeed, the signal of water molecules' vibrations is a very broad cluster peak: a doublet with two maxima, one at 1650 cm^{-1} corresponding to one of three O-H bond vibrational modes, here the OH bending, and the other around 1400cm^{-1} indicating the presence of Hydrogen Bonds (HB) between water molecules [22]. In H-ND suspensions, the observed water signal in Raman spectrum is highly affected by the presence of H-ND as shown in (Figure 1). Surprisingly, the intensity of O-H bending signal at 1650cm^{-1}, as well as the signal corresponding to HBs at 1400 cm^{-1} are weaker for H-ND suspensions than for water alone. Moreover, the intensity of the O-H bending line at 1650cm^{-1} becomes less intense than that of the HB at 1400cm^{-1} in presence of H-ND. Moreover, the intensity bias of these two spectral lines is contrary to what is observed in the case of water alone. This spectral behavior confirms an interaction between water molecules and H-ND surface, which impacts water molecules organization in the suspension.

A chaotropic agent, such as DMSO [29] is capable of disrupting [30] hydrogen bonds network, which are structuring the liquid water [31,32]. DMSO can, in fact, only be an acceptor of HB, whereas water is both an acceptor and a donor [33]. Indeed, we have observed by Raman analysis, starting from 3% (v/v) DMSO in water, alterations in vibrational intensities of O-H bonds. These alterations are seen as a decrease of water signal intensity around the area of 1330 cm^{-1} as a function of DMSO percentage. This signal is greatly reduced and no more detectable at 12% and 50% (v/v) DMSO in water, respectively (Figure 2).

Consequently, in order to minimize this masking effect of the water signal, different concentrations of H-ND were put in a suspension in water containing increasing concentrations of DMSO (5%, 12% and 50% (v/v) DMSO in water). The C-C sp^3 diamond line is not discretely identifiable in suspensions, however when analyzing the H-ND suspensions with increasing concentrations, spectral

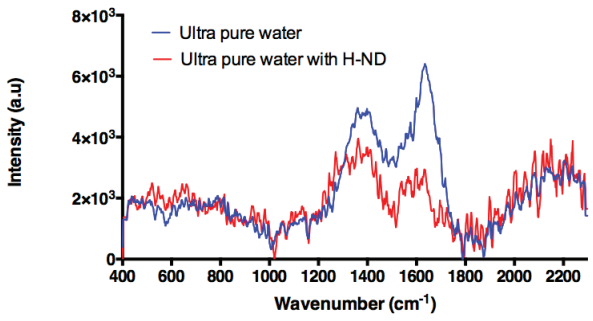

Figure 1: Ultra-pure water Raman Spectrum (in blue) and Raman spectrum of 1.8 mg/ml of H-ND aqueous suspension (In red).

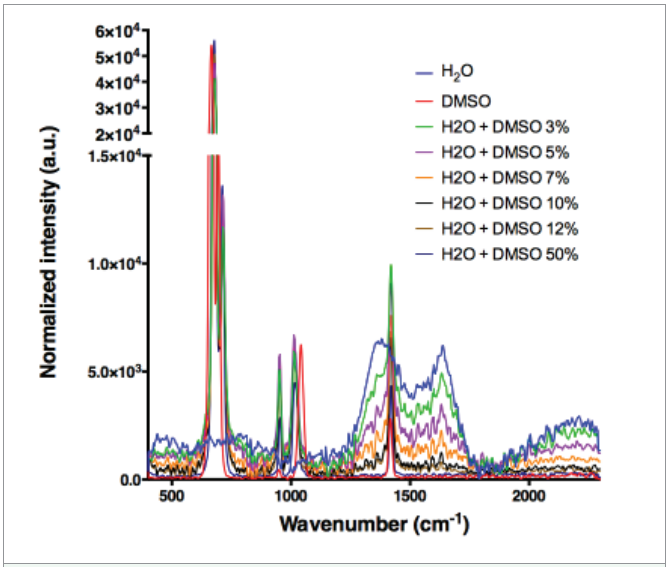

Figure 2: Raman Spectra of different DMSO concentrations in water solutions.

intensities in the area around 1330 cm^{-1} increase with the H-ND suspensions' concentration, in all analyzed DMSO concentration (Figures 3a, 3b, 3c).

Therefore, it was crucial to investigate the potential proportionality between the peak intensities and the variations of H-ND suspensions' concentrations in this area. The observed intensities in the given area have been normalized with the DMSO methyl group peak intensity at 950cm^{-1} [34]. For each frequency in the spectral region between 1200cm^{-1} and 1400cm^{-1}, the linearity regression factor has been calculated, in reference to the H-ND concentration. For each of analyzed DMSO concentrations, the five highest linear regression factors have been selected using a ranking method to determine discrete frequencies' values (Table 1).

For H-ND suspensions in 5% and 50% (v/v) DMSO in water, the correlations are weak. More precisely for 5% (v/v) DMSO, we observe in figure 4a a linear dependence for low H-ND concentrations, whereas above H-ND suspension concentration of 300µg/ml, the signal becomes saturated. For 50% (v/v) DMSO in water, there is no linearity for lower H-ND concentrations (Figure 4c). However, around the H-ND concentration of 180µg/ml and above, the signal becomes linear. On the other hand, for H-ND suspensions in 12% (v/v) DMSO in water, as presented in figure 4b, the linearity regression factors calculated in the same manner, present a strong correlation between 0.993 and 0.978 for the five selected frequencies, all found between 1226 cm^{-1} and 1348 cm^{-1}, as shown in table 1, section B. These factors indicate the proportionality between H-ND concentrations and the observed signal for the five selected frequencies. This fact confirms the possibility of H-ND quantification in aqueous suspensions in 12% (v/v) DMSO in water. Regardless of the DMSO concentration, all the signals presenting the best correlations are found between 1226 cm^{-1} and 1348 cm^{-1}. For the tested H-ND batches, the conditions 1) 12% (v/v) DMSO in water and 2) 1230 cm^{-1} a calibration curve is obtained for evaluation of H-ND suspension concentrations. The correlation factor of 0.993 allows an estimation with less than 1% of error probability. However, a calibration curve has to be realized each time for a new type of particles when their parameters change; more precisely, the hydrogenation ratio of the H-ND surface and their size distribution, since these are the parameters essential for a Raman response.

The DMSO has been used in suspensions' analyses to potentially unveil the C-C sp^3 diamond signal by clearing off the masking water signal in the same region. We had to verify then, if one of these signals represents the displaced C-C sp^3 diamond line, knowing that the signal may be affected by various experimental factors, such as the excitation laser, the solvent [35] etc. For this premise to be true, this signal's distinction should presumably increase with the increasing DMSO concentration in suspensions, however, this is not what we observe when comparing the signals of H-ND suspensions in 12% and 50% (v/v) DMSO in water. This absence of signal distinction is a

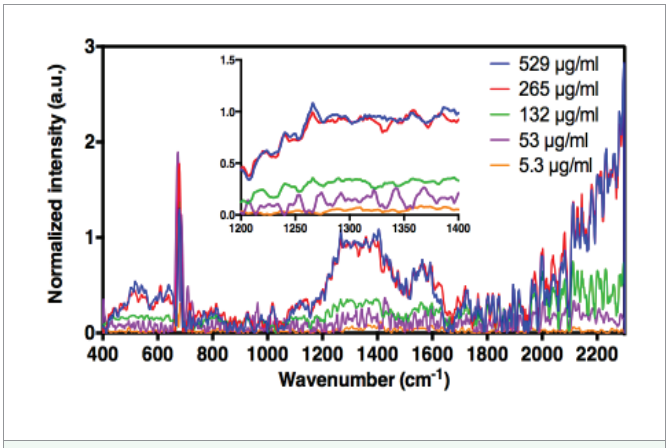

Figure 3a: Raman Spectra of H-ND suspensions in 5% DMSO v/v in water.

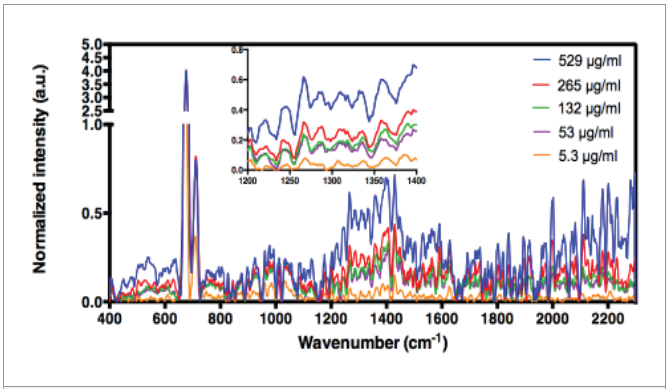

Figure 3b: Raman Spectra of H-ND suspensions in 12% DMSO v/v in water.

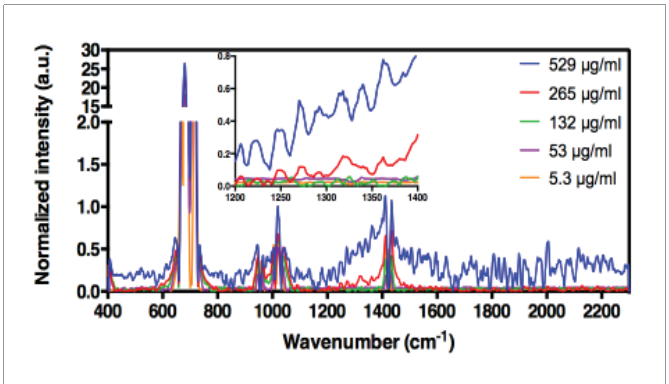

Figure 3c: Raman Spectra of H-ND suspensions in 50% DMSO v/v in water.

	% DMSO in H_2O	Wavenumber (cm^{-1})	Concentrations & Intensities					Linearity regression factors
			529 µg/ml	265 µg/ml	132 µg/ml	53 µg/ml	5.3 µg/ml	R^2
A	5	1226	0.66691	0.61711	0.23156	0.15608	0.07573	84.9%
		1228	0.67757	0.65576	0.26604	0.18404	0.09966	82.3%
		1230	0.69743	0.68219	0.28161	0.21052	0.10466	81.5%
		1232	0.66728	0.63958	0.23970	0.15756	0.08716	82.8%
		1348	1.06250	1.03733	0.44277	0.29476	0.18378	81.9%
B	12	1226	0.28592	0.15035	0.10826	0.09323	0.05445	98.1%
		1228	0.26408	0.13432	0.09676	0.07303	0.04391	98.7%
		1230	0.26264	0.13432	0.09732	0.05968	0.03622	99.3%
		1232	0.25230	0.11287	0.08054	0.04430	0.02656	98.5%
		1348	0.39943	0.20472	0.15164	0.12234	0.05247	97.8%
C	50	1226	0.20342	0.05418	0.03407	0.01251	0.03441	87.3%
		1228	0.28845	0.09217	0.03010	0.01132	0.03398	91.7%
		1230	0.31957	0.09882	0.03742	0.01102	0.03441	92.1%
		1232	0.23739	0.07058	0.02968	0.01013	0.03441	89.7%
		1348	0.51993	0.13556	0.03679	0.01310	0.03398	91.2%

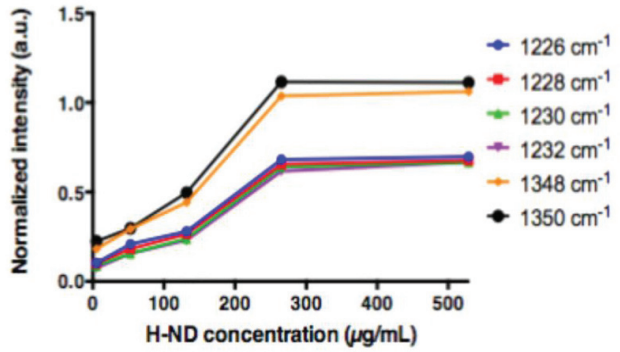

Figure 4a: Raman signal dependence on H-ND suspensions concentrations for each selected frequency at 5% DMSO in water.

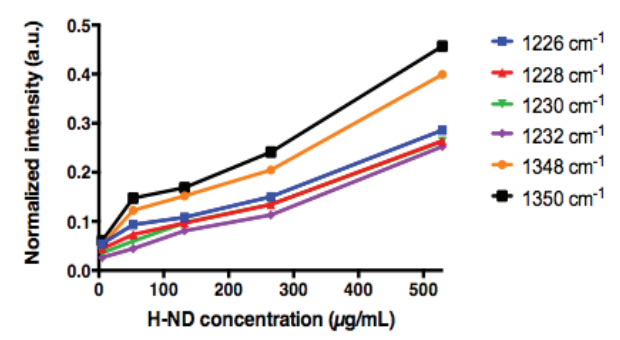

Figure 4b: Raman signal dependence on H-ND suspensions concentrations for each selected frequency at 12% DMSO in water.

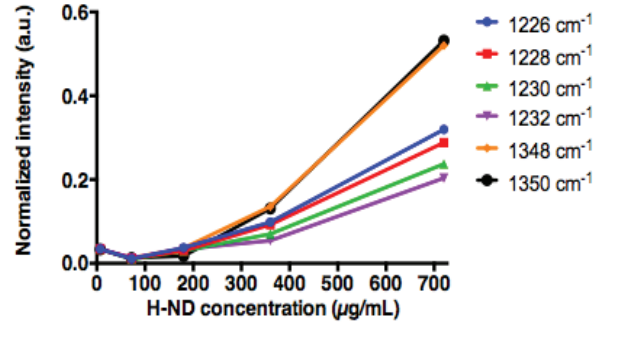

Figure 4c: Raman signal dependence on H-ND suspensions concentrations for each selected frequency at 50% DMSO in water.

direct consequence of a larger number of disrupted HB in the water network with 50% DMSO than that in the case of the 12% DMSO, which suggests that none of the five selected frequencies correspond to the C-C sp^3 diamond vibrational signal. Nonetheless, in the experiment with H-ND in pure DMSO, there is no significant signal in the observed region. However, the loss of this signal is reversible if diluting the DMSO with water to reach 12% (v/v) DMSO in water, which implies that there is no irreversible chemical reaction between DMSO and H-ND.

By widening the spectral window from 1200 - 1400 cm^{-1} to 1200-1800cm^{-1}, the latter corresponding to the area of vibrations of water molecules (O-H bending and HB), the calculated linearity regression factors highlight other frequencies around 1700 cm^{-1} where the intensities are strongly correlated with H-ND concentrations. Low distinction of these signals in suspensions with high DMSO

concentration rules out the probability of a C-C sp^2 vibrational signal presence.

Since the signal we observe does not correspond to the C-C sp^3 or the C-C sp^2 signal, the question remains, to what does this signal truly correspond? It seems that in H-ND aqueous colloidal suspensions, at least two types of interactions with different energies coincide; type 1: between the solvent and the H-ND at the interface and type 2: the interaction between the molecules of the rest of the solvent, as suggested by Petit, et al. [36]. While the HB between DMSO and water are stronger than those between water molecules solely [33] and because the water molecules bonded to H-ND at the interface cannot be removed by 12% (v/v) DMSO in water, this implies that the interactions between H-ND and the first hydration shell might be even stronger than those between DMSO and water. These facts suggest that what allows H-ND quantification are in fact, water molecules strongly interacting with H-ND [15], which the DMSO at 12%, is not able to remove. To verify this, the H-ND suspensions in water or in 12% (v/v) DMSO in water, have been tested in a series of phase exchange experiments, wherein, these suspensions were not able to cross aliphatic-aqueous or aqueous-perfluoroalkane interfaces, respectively, despite the density differences, even when centrifuged [37]. We have observed that the H-ND (density of 3,75g/cm^3), in a suspension with a pure aliphatic phase, like oil (density of 0,9g/cm^3) are not able to cross the oil-water (density of 1g/cm^3) interface, even with centrifugation. This confirms the lipophilic nature of H-ND surface in the case where H-ND have not previously been in contact with water. On the other hand, H-ND, in a suspension either with pure water or with 12% (v/v) DMSO in water, are not able to cross the interface water-tetradecafluorohexane, whose density is of 1.7g/cm^3, even with centrifugation. On the contrary, dry H-ND migrate across the tetradecafluorohexane phase. In conclusion, the molecules providing the solvation of H-ND are tightly bound to H-ND and cannot be removed by an amphiphobic environment such as perfluoroalkanes. From the moment when the H-ND have been put in contact with water, a durable hydration shell forms, indicating the hydrophilic nature of H-ND. The interaction type between the H-ND and the solvent seems to be very important, since it defines their organization and structural stability. The importance here is to clarify if the observed interaction between the H-ND and the water molecules is a result of a direct interaction; HB, Van der Waals, electrostatic interactions or is it indirect such as a formation of a hydrophobic pocket or gap. Two major hypotheses may serve as an explanation of these interactions: an indirect cage-type interaction [38] or a direct bond with H-ND.

The model of Petit, et al. [36] proposes the solvation of H-ND by their capacity of electron accumulation on the surface. This model implies necessarily that the electron layer has to be stabilized with water molecules oriented with their hydrogen atoms towards the H-ND surface. These stabilizing water molecules form a tetrahedral ice-like network of Double Donors (DD) and Double Acceptors (AA). Verifying the H-ND solvation in a solvent, which does not allow DD and AA bonds, would help making a choice between the two hypotheses. To answer this question, water has been substituted by ethanol where oxygen atom has two doublets capable of accepting HBs but has only one hydrogen atom as a donor, making impossible the network formation of DD and AA solvent organization [39]. When a suspension of H-ND in ethanol is put on top of an oil phase, the H-ND do not cross to the oil phase, certainly due to the ethanol solvation of the H-ND (Illustration in figure 5).

Moreover, to respect the same conditions as for the suspensions of H-ND in 12% (v/v) DMSO in water, we have analyzed H-ND in 12% (v/v) DMSO in ethanol. The ethanol spectrum profile limits the observation window of frequencies to 1200-1250cm^{-1}, 1300-1350cm^{-1} and 1550-1800cm^{-1}. Nevertheless, for these observed windows we obtain a linear dependence between the H-ND suspension concentrations in 12% (v/v) DMSO in ethanol and the frequencies in these zones as presented in figure 6.

Furthermore, this solvation of H-ND by ethanol, does not involve a system of HB like DD in the solvent molecules. This means that in the model with electron accumulation on the H-ND surface [36], ethanol molecules would not be capable to stabilize this kind of system. According to our results, for the above said, the most probable possibility is a HB between H-ND and ethanol. However, a physisorption could occur, where the aliphatic groups of ethanol adsorb onto H-ND surface and on that account allows solvation by ethanol [40]. This scenario is highly improbable, since the H-ND do not aggregate in ethanol and are not capable of crossing the ethanol-oil interface as shown in figure 7.

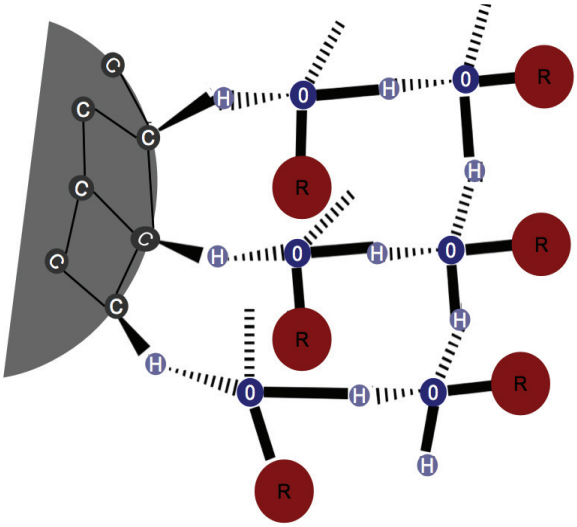

Figure 5: An example of ethanol molecule organization around a H-ND. Formation of HB network, on one side between the hydrogen atom on the H-ND surface and a doublet of the oxygen atom of the ethanol, and on the other side between a hydrogen and the oxygen in ethanol.

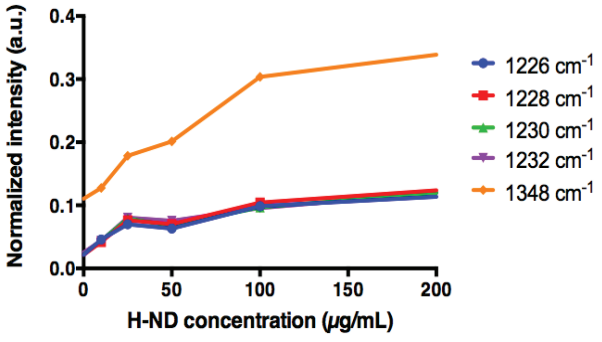

Figure 6: Raman signal dependence on H-ND suspensions concentrations for each selected frequency at 12% DMSO v/v in ethanol.

The core of an H-ND is formed of C-C bonds, consequentially, there is a difference in potential, sufficient to induce a C-H bond polarization with the surface charge distribution, δ- on the carbon atom and δ+ on the hydrogen atom, as illustrated in the figure 8. This phenomenon is possible even for the C-H bonds involved in eventual C-C sp^2 bonds potentially present on the H-ND surface. This difference in potential would allow a formation of a HB between the hydrogen atom on the H-ND surface and the oxygen atom of the water.

To verify the possibility of a HB, we have analyzed H-ND suspensions in pure DMSO, the latter being only an AA, the only possible HB could be formed between the hydrogen atom of H-ND and the oxygen atom of the DMSO. In figure 2, as already reported for DMSO solutions in water, we observe that the sulfoxide group (S = O) peak of DMSO at 1046 cm^{-1} is displaced to a lower vibration at 1012 cm^{-1} (a red shift) with the difference of 10 cm^{-1} in the Full Width at Half Maximum (FWHM) of the peak, demonstrating the presence of a HB between the oxygen atom of the DMSO and the hydrogen atom from the water molecule [17]. Moreover, this S = O peak intensity, increases in a non-linear fashion, related to the DMSO concentration in water, as expected for a DD [41], such as presented in figure 9.

If we analyze Raman spectra of increasing H-ND suspensions concentrations in pure DMSO, a similar phenomenon occurs, a red shift of the S = O vibrational signal with the difference of 16 cm^{-1} in the FWHM, and a non-linear increase of the signal with the increasing H-ND concentrations, as shown in figure 10, directly proving a HB formation.

While the carbon's electronegativity is 2.55 and 3.45 for the oxygen, we could expect weak HB between H-ND and water. However, 12% (v/v) DMSO in water is not capable of destroying these bonds while it disrupts those linking water molecules. Based on the structure of clusters' hydration (as in happens with methanol), where the clusters form HB with water molecules [42] and based on the observations of the existence of a cage-type structure of water molecules surrounding the H-ND as described by Petit, et al. [36] in the X-ray Absorption (XAS) spectrum [38], we may deduce that the HB between H-ND and water are stabilized by a cage-type water

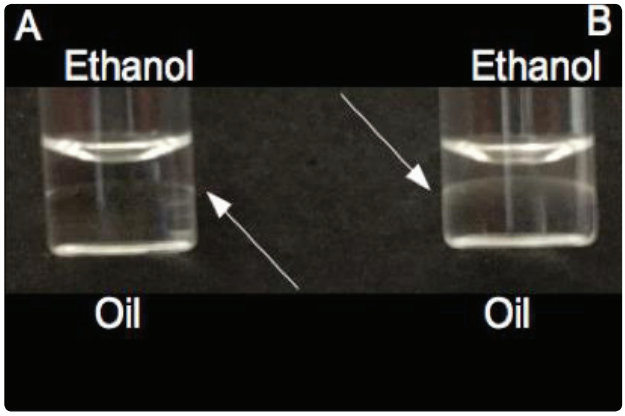

Figure 7: A: Ethanol/oil interface after centrifugation. B: H-ND on the ethanol/oil interface, after centrifugation

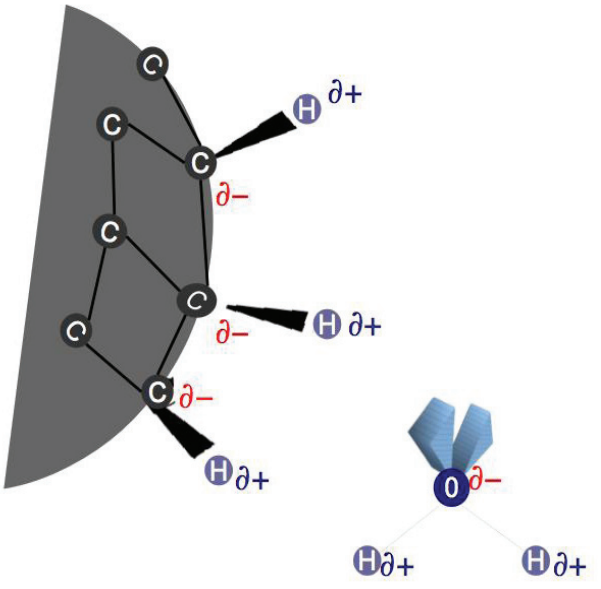

Figure 8: Example of a partial ionization of σ bonds between a hydrogen and a sp^3 carbon of the H-ND, bound to three other carbon atoms. (An ionization of the σ bond may also exist between a hydrogen and a sp^2 carbon).

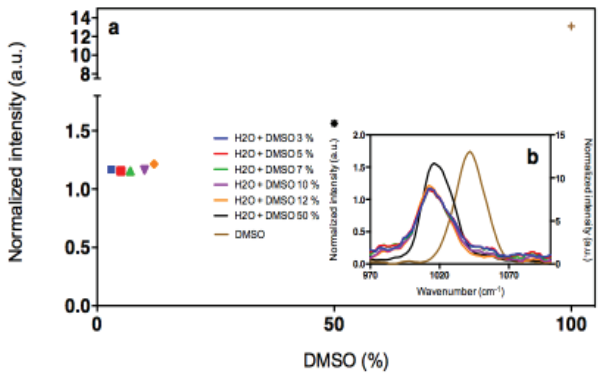

Figure 9: Dependence of the S = O peak on different percentages of DMSO in water.
a: Non linear evolution of the peak intensity relative to DMSO percentage. b: Red shift of the S = O peak

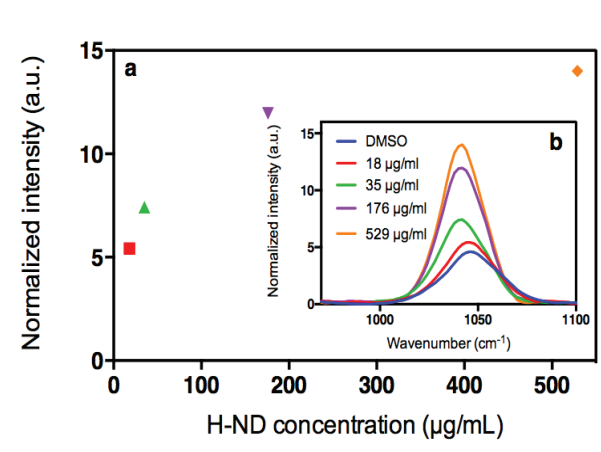

Figure 10: Dependence of the S = O peak on H-ND concentration in pure DMSO.
a: Non linear evolution of the S = O peak intensity
b: Red shift of the S = O peak

organization. This would explain their great stability allowing the whole structure to resist to 12% (v/v) DMSO in water. The described structure is a result of the ambivalent behavior of the H-ND regarding their lipophilic and hydrophilic nature. The lipophilic aspect tends to disrupt the water molecules' network. However, in order to minimize this perturbation, water molecules may contract weak HB with a slightly polarized hydrogen on the H-ND surface, forming around the H-ND a network of HB between the water molecules, which stabilize these weak HB and allow efficient hydration of the particle (Illustrated in figure 11).

CONCLUSION

Throughout this study, we have developed a technique based on Raman spectroscopy that provides insights to the water interaction with H-ND. We have shown that the solvation of the H-ND is carried out through HB involving directly water molecules in the hydration shell. These HB have been identified as particular bonds, implying the hydrogen atom of H-ND as a HB donor and a doublet on the oxygen atom in a water molecule as an acceptor. This organization explains the formation of a hydration shell creating an intrinsically stable system. This type of hydration has already been reported for macromolecules such as DNA [42-44] or proteins [45-47], and the similarity of these systems' hydration to H-ND hydration is not surprising at all, seen the size and the surface functionality of these macromolecules. We have demonstrated a linear evolution of the Raman signal of water molecules bound to H-ND, depending on the H-ND suspensions concentrations. Further, this approach suggests that the quantification of water molecules strongly bonded to the H-ND would allow a direct quantification of H-ND in aqueous suspensions. To do this, we have shown the efficiency of DMSO as an agent blurring the free water signal, which allows highlighting bound water in the Raman spectral region between 1200 cm^{-1} and 1800 cm^{-1}. Since the H-ND are currently used in research as a radio-sensitizing tool [3], the direct H-ND quantification in aqueous suspensions is of great interest for biological and biomedical applications.

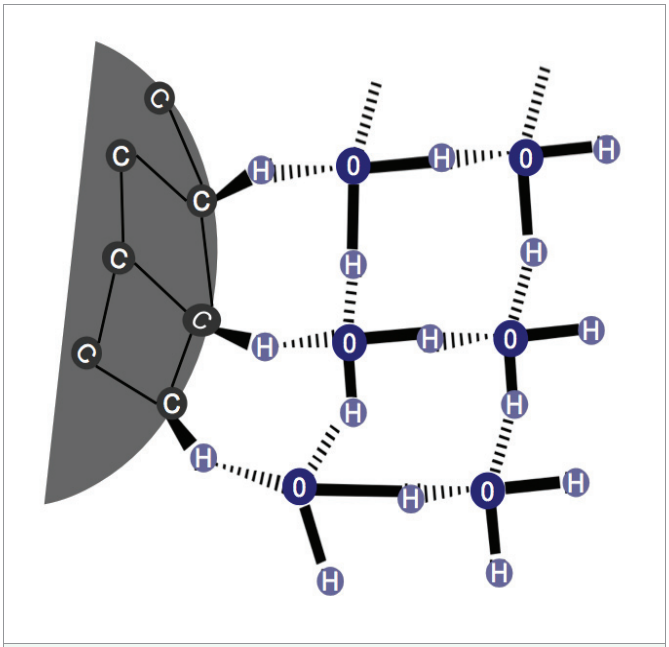

Figure 11: An example of water molecules' organization around a H-ND. Formation of a network of HB: on one side between a hydrogen atom on the H-ND surface and a doublet of the oxygen atom from a water molecule and on the other side, between the water molecules themselves.

ACKNOWLEDGEMENT

This work was funded by the French National Research program INDIRA project (INDIRA-11RSNR0011). The authors thank Prof. Oliver A Williams from Cardiff Diamond Foundry, School of Physics and Astronomy, Cardiff University as well as Dr. Jean-Charles Arnault and Dr. Hugues Girard form Diamond Sensors Laboratory, CEA, LIST, for having kindly provided the hydrogenated nanodiamond suspension samples for this work.

REFERENCES

1. Wang T, Handschuh-Wang S, Qin P, Yang Y, Zhou X, Tang Y. Enhancing the colloidal stability of detonation synthesized diamond particles in aqueous solutions by adsorbing organic mono-, bi- and tridentate molecules. J Colloid Interface Sci. 2017; 499: 102-109. **PubMed**. https://www.ncbi.nlm.nih.gov/pubmed/28364714

2. Mikhail VK, Dmitry SV, Natalya VA, Belyaeva A, Pavel IS, Mikhail AP. Improving the dispersity of detonation nanodiamond: Differential scanning calorimetry as a new method of controlling the aggregation state of nanodiamond powders. Nanoscale. 2013; 5: 1529. https://rsc.li/2EpvU3P

3. Grall R, Girard H, Saad L, Petit T, Gesset C, Combis-Schlumberger M, et al. Impairing the radioresistance of cancer cells by hydrogenated nanodiamonds. Biomaterials. 2015; 61: 290-298. **PubMed:** https://www.ncbi.nlm.nih.gov/pubmed/26010122

4. Paget V, Sergent JA, Grall R, Altmeyer-Morel S, Girard HA, Petit T, et al. Carboxylated nanodiamonds are neither cytotoxic nor genotoxic on liver, kidney, intestine and lung human cell lines. Nanotoxicology. 2014; 8: 46-56. **PubMed:** https://www.ncbi.nlm.nih.gov/pubmed/24266793

5. Oliver AW, Jakob Hees, Christel Dieker, Wolfgang Jäger, Lutz Kirste, Christoph EN. Size-dependent reactivity of diamond nanoparticles. ACS Nano. 2010; 4: 4824-4830. https://bit.ly/2srw3k8

6. Ho D, Wang CH, Chow EK. Nanodiamonds: The intersection of nanotechnology, drug development and personalized medicine. Sci Adv. 2015; 21: e1500439-e1500439. **PubMed:** https://www.ncbi.nlm.nih.gov/pubmed/26601235

7. Mochalin VN, Shenderova O, Ho D, Gogotsi Y. The properties and applications of nanodiamonds. Nat Nanotechnol. 2011; 7: 11-23. **PubMed:** https://www.ncbi.nlm.nih.gov/pubmed/22179567

8. Chao JI, Perevedentseva E, HuaChung P, KaiLiu K, YuanCheng C, ChingChang C, et al. Nanometer-sized diamond particle as a probe for bio labeling. Biophys Journal. 2007; 93: 2199-2208. http://bit.ly/36w0PqX

9. Tristan P, Hugues AG, Adeline T, Isabelle BG, Philippe B, Jean-CA. Surface transfer doping can mediate both colloidal stability and self-assembly of nanodiamonds. Nanoscale. 2013; 5: 8958. https://rsc.li/36zfu4y

10. Turcheniuk K, Mochalin VN. Biomedical applications of nanodiamond (Review). Nanotechnology. 2017; 28. 252001. **PubMed:** https://www.ncbi.nlm.nih.gov/pubmed/28368852

11. JC Arnault. Nanodiamonds advanced material analysis, properties and applications. Nanodiamonds 1st Edition. Elsevier. 2017. http://bit.ly/2Pj4jYj

12. Shenderova, Hens S, McGuire G. Seeding slurries based on detonation nanodiamond in DMSO. Diam Relat Mater. 2010; 19: 260-267. http://bit.ly/2RNGA3X

13. Ji S, Jiang T, Xu K, Li S. FTIR study of the adsorption of water on ultradispersed diamond powder surface. Appl Surf Sci. 1998; 133: 231-238. http://bit.ly/2Egtuo0

14. Girard HA, Petit T, Perruchas S, Gacoin T, Gesset C, Arnault JC, et al. Surface properties of hydrogenated nanodiamonds: A chemical investigation. Phys Chem Chem Phys. 2011; 13: 11517-11523. **PubMed:** https://www.ncbi.nlm.nih.gov/pubmed/21566816

15. Stehlik S, Glatzel T, Pichot V, Pawlak R, Meyer E, Spitzer D, et al. Water interaction with hydrogenated and oxidized detonation nanodiamonds - Microscopic and spectroscopic analyses. Diam Relat Mater. 2016; 63: 97-102. http://bit.ly/2rIbTCG

16. Dolenko TA, Burikov SA, Rosenholm JM, Shenderova OA, Vlasov II.

Diamond-water coupling effects in raman and photoluminescence spectra of nanodiamond colloidal suspensions. J Phys Chem. 2012; 116: 24314-24319. http://bit.ly/2tag7Dj

17. Scherer JR, Go MK, Kint S. Raman spectra and structure of water in dimethyl sulfoxide. J Phys Chem. 1973; 77: 2108-2117. http://bit.ly/2LRDYhM

18. Bogdanov KV, Osipov VY, Zhukovskaya MV, Jentgens C, Treussart F, Hayashi T, et al. Size-dependent raman and SiV-center luminescence in polycrystalline nanodiamonds produced by shock wave synthesis. RSC Adv. 2016; 6: 51783-51790. https://rsc.li/34i700n

19. Stehlik S, Varga M, Ledinsky M, Jirasek V, Artemenko A, Kozak H, et al. Size and purity control of HPHT nanodiamonds down to 1 nm. J Phys Chem C Nanomater Interfaces. 2015; 119: 27708-27720. **PubMed:** https://www.ncbi.nlm.nih.gov/pubmed/26691647

20. Yuan Y, Chen Y, Liu JH, Wang H, Liu Y. Biodistribution and fate of nanodiamonds in vivo. Diam Relat Mater. 2009; 18: 95-100. http://bit.ly/2PgpPg4

21. Sun KW, Wang JY, Ko TY. Raman spectroscopy of single nanodiamond: Phonon-confinement effects. Appl Phys Lett. 2008; 92: 153115. https://bit.ly/34q17Ow

22. Bratos S, Leicknam J Cl, Gallot G, Ratajczak H. Infra-Red spectra of hydrogen bonded systems: Theory and experiment. 2002; 5-30. https://bit.ly/34oMV8z

23. Ahmed M, Singh AK, Mondal JA. Hydrogen-bonding and vibrational coupling of water in a hydrophobic hydration shell as observed by Raman-MCR and isotopic dilution spectroscopy. Phys Chem Chem Phys. 2016; 18: 2767-2775. **PubMed:** https://www.ncbi.nlm.nih.gov/pubmed/26725484

24. Jong Min Park, Cheol Jun Song, Wang Yao, Chang Young Jung, In Ho Hyun, Dong Hoon Seong, et al. Synthesis of carbohydrate-conjugated azaphthalocyanine complexes for PDT. Tetrahedron Lett. 2015; 56: 4967-4970. https://bit.ly/36GTsgi

25. Vadym Mochalin, Sebastian Osswald, Yury Gogotsi. Contribution of functional groups to the raman spectrum of nanodiamond powders. Chem Mater. 2009; 21: 273-279. https://bit.ly/34r0QLi

26. Michel Mermoux, Alexandre Crisci, Tristan Petit, Hugues A Girard, Jean-Charles Arnault. Surface modifications of detonation nanodiamonds probed by multiwavelength raman spectroscopy. J Phys Chem C. 2014; 118: 23415-23425. https://bit.ly/2PQIWMO

27. Aleksenskii AE, Baidakova MV, Vul A Ya, Davydov V Yu, Pevtsova Yu A. Diamond-graphite phase transition in ultradisperse-diamond clusters. Phys Solid State. 1997; 39: 1007-1015. https://bit.ly/35lkauR

28. Yoshikawa M, Mori Y, Obata H, Maegawa M, Katagiri G, Ishida H, Ishitani A. Raman scattering from nanometer sized diamond. Appl Phys Lett.1995; 67: 694-696. https://bit.ly/2YYPYU4

29. Vaclav Vetvicka, Miroslav Novak. Beta-Glucan, structure, chemistry and specific application. Bentham Science Publishers. 2013; 2. https://bit.ly/2tf7U0G

30. Alenka Luzar, David Chandler. Structure and hydrogen bond dynamics of water-dimethyl sulfoxide mixtures by computer simulations. J Chem Phys. 1993; 98: 8160-8173. https://bit.ly/2YSBy7Q

31. Sotiris S Xantheas. Cooperativity and hydrogen bonding network in water clusters. Chem Phys. 2000; 258: 225-231. https://bit.ly/2PnNT0w

32. Paul C Cross, John Burnham, Philip A Leighton. The raman spectrum and the structure of water. J Am Chem Soc. 1937; 59: 1134-1147. https://bit.ly/2Q1Tmtl

33. Brayton CF. Dimethyl Sulfoxide (DMSO): a review. Cornell Vet. 1986; 76: 61-90. **PubMed:** https://www.ncbi.nlm.nih.gov/pubmed/3510103

34. Selvarajan. Raman spectrum of Dimethyl Sulfoxide (DMSO) and the influence of solvents. Proc Indian Acad Sci-Sect A. 1966; 64: 44-50. https://bit.ly/38DUV9j

35. Giorgini MG, Musso M, Torii H. Concentration-dependent frequency shifts and raman spectroscopic noncoincidence effect of the C = O stretching mode in dipolar mixtures of acetone/dimethyl sulfoxide. Experimental, theoretical, and simulation results. J Phys Chem A. 2005; 109: 5846-5854. https://bit.ly/2POi3Jt

36. Tristan Petit, Ljiljana Puskar, Tatiana Dolenko, Sneha Choudhury, Eglof Ritter, Sergey Burikov, et al. Unusual water hydrogen bond network around hydrogenated nanodiamonds. J Phys Chem C. 2017; 121: 5185-5194. https://bit.ly/2YQQvY1

37. Moore FG, Richmond GL. Integration or Segregation: How do molecules behave at oil/water interfaces?, Acc Chem Res. 2008; 41: 739-748. **PubMed:** https://www.ncbi.nlm.nih.gov/pubmed/18507401

38. Tristan Petit, Hayato Yuzawa, Masanari Nagasaka, Ryoko Yamanoi, Eiji Osawa, Nobuhiro Kosug, et al. Probing interfacial water on nanodiamonds in colloidal dispersion. J Phys Chem Lett. 2015; 6: 2909-2912. https://bit.ly/2PNhdwt

39. Sergey Burikov, Tatiana Dolenko, Svetlana Patsaeva, Yuriy Starokurov, Viktor Yuzhakov. Raman and IR spectroscopy research on hydrogen bonding in water-ethanol systems. Mol Phys. 2010; 108: 2427-2436. https://bit.ly/2RWUTDw

40. Nagasaka M, Mochizuki K, Leloup V, Kosugi N. Local structures of methanol-water binary solutions studied by soft x-ray absorption spectroscopy. J Phys Chem B. 2014; 118: 4388-4396. **PubMed:** https://www.ncbi.nlm.nih.gov/pubmed/24694018

41. Dixit S, Crain J, Poon WC, Finney JL, Soper AK. Molecular segregation observed in a concentrated alcohol-water solution. Nature. 2002; 416: 829-832. **PubMed:** https://www.ncbi.nlm.nih.gov/pubmed/11976678

42. Betaa A, Michalarias I, Ford RC, Li JC, Bellissent-Funel BC. Quasi-elastic neutron scattering study of hydrated DNA. Chem Phys. 2003; 292: 451-454. https://bit.ly/36EMh8q

43. Cecilia Leal, Lars Wadso, Gerd Olofsson, Maria Miguel, Hakan Wennerstrom. The hydration of a DNA-Amphiphile complex. J Phys Chem B. 2004; 108: 3044-3050. https://bit.ly/2PTowCO

44. Soler-López M, Malinina L, Subirana JA. Solvent organization in an oligonucleotide crystal. J Biol Chem. 2000; 275: 23034-23044.

45. Adam Hospital, Michela Candotti, Josep Lluís Gelpí, Modesto Orozco. The multiple roles of waters in protein solvation. J Phys Chem B. 2017; 121: 3636-3643. https://bit.ly/2RVE0ck

46. Martinianoa HFMC, Galamba N. Fast and slow dynamics and the local structure of liquid and supercooled water next to a hydrophobic amino acid. Phys Chem Chemical Phys. 2016; 18: 27639-27647. https://rsc.li/2rOL4wF

47. Laage D, Elsaesser T, Hynes JT. Water Dynamics in the hydration shells of biomolecules. Chem Rev. 2017; 117: 10694-10725. **PubMed:** https://www.ncbi.nlm.nih.gov/pubmed/28248491